

Bridging Synthetic and Real Worlds for Pre-training Scene Text Detectors

Tongkun Guan, Wei Shen[✉], Xue Yang, Xuehui Wang, Xiaokang Yang
MoE Key Lab of Artificial Intelligence, AI Institute, Shanghai Jiao Tong University

{gtk0615, wei.shen}@sjtu.edu.cn

Abstract

Existing scene text detection methods typically rely on extensive real data for training. Due to the lack of annotated real images, recent works have attempted to exploit large-scale labeled synthetic data (LSD) for pre-training text detectors. However, a synth-to-real domain gap emerges, further limiting the performance of text detectors. Differently, in this work, we propose *FreeReal*, a real-domain-aligned pre-training paradigm that enables the complementary strengths of both LSD and unlabeled real data (URD). Specifically, to bridge real and synthetic worlds for pre-training, a glyph-based mixing mechanism (*GlyphMix*) is tailored for text images. *GlyphMix* delineates the character structures of synthetic images and embeds them as graffiti-like units onto real images. Without introducing real domain drift, *GlyphMix* freely yields real-world images with annotations derived from synthetic labels. Furthermore, when given free fine-grained synthetic labels, *GlyphMix* can effectively bridge the linguistic domain gap stemming from English-dominated LSD to URD in various languages. Without bells and whistles, *FreeReal* achieves average gains of 1.59%, 1.97%, 3.90%, 3.85%, and 4.56% in improving the performance of *DPTText*, *FCENet*, *PSENet*, *PANet*, and *DBNet* methods, respectively, consistently outperforming previous pre-training methods by a substantial margin across four public datasets. Code will be released soon.

1. Introduction

Scene text detection aims to predict the bounding box or polygon for each arbitrarily shaped text instance within an image. This technology has diverse applications, including online education, instant translation, and product search, owing to the prevalence of text-laden images. However, despite their considerable progress, supervised methods [8, 20, 41, 45, 62] still struggle with an increasing demand for real data with labor-intensive annotations, especially when detecting complicated text images.

In contrast, recent research efforts [35, 38, 48] have focused on pre-training scene text detectors using large-scale

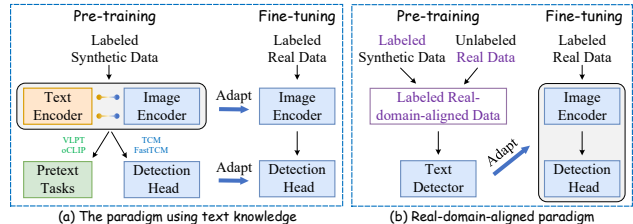


Figure 1. We present different pre-training paradigms for enhancing text detectors. (a) represents the existing pre-training paradigm by leveraging visual and textual knowledge. (b) denotes our paradigm by leveraging the intrinsic qualities of real-world unlabeled images with annotations derived from synthetic labels.

labeled synthetic data (LSD), which leverage both visual and textual knowledge to extract text feature representations, as illustrated in Fig. 1(a). For example, VLPT [35] formulates three cross-modality pretext tasks to enhance the performance of the backbone, and oCLIP [48] focuses on aligning visual and textual information to assist text detectors. Nevertheless, these well-curated designs are limited to using synthetic images due to their reliance on labeled word transcriptions. This limitation will lead to a noticeable synth-to-real domain gap when models are fine-tuned on real data, negatively impacting text detection performance. Therefore, exploring the potential of unlabeled real data (URD) is of great importance as they are readily available. However, the pre-training on URD has seldom been studied. One of the few works [40] attempts to pre-train text detectors on URD via masked image modeling [12] (step 1) and on LSD via supervised learning (step 2), which will re-transfers pre-trained weights from the real domain to the synthetic domain.

Differently, our objective is to jointly leverage LSD and URD by bridging their gap for enhancing the text detector pre-training, as shown in Fig. 1(b). The primary challenge is how to effectively modulate these URD and LSD without encountering real domain drift. In light of this, we initially investigate the adaptation capabilities of existing domain-bridging methods [30, 57, 60]. This involves training a classifier to distinguish between URD and LSD and subsequently assessing the confidence of these domain-bridging

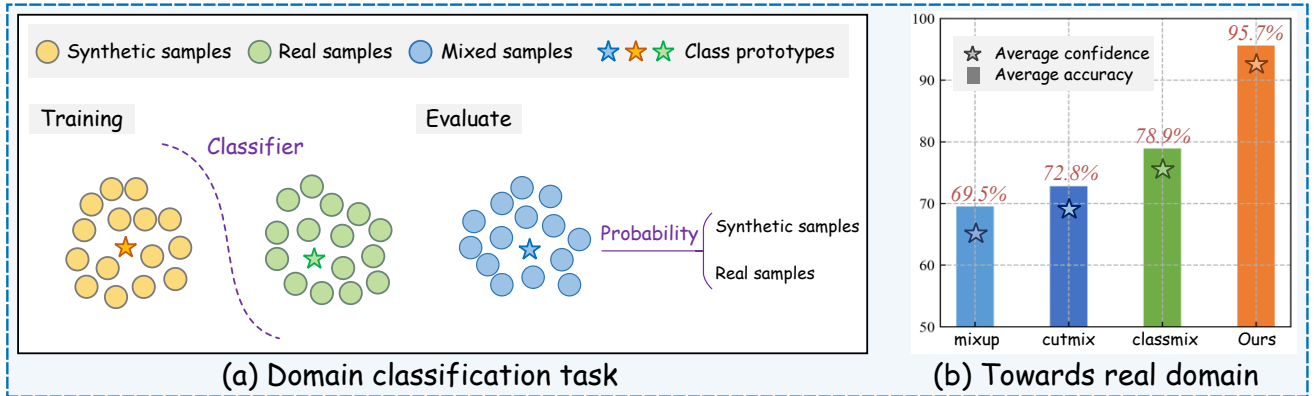


Figure 2. We present the domain classification task and the performances of different domain bridging ways between LSD and URD. In the text detection area, experiments demonstrate that our domain bridging method significantly performs better in aligning with the real domain. This is easy to explain: (I) Mixup may lead to unexpected pixel-wise ambiguities; (II) CutMix may cause the absence of many text regions and incomplete semantics of texts; (III) ClassMix will introduce salient boundary priors; (IV) GlyphMix (ours) effectively preserves the semantic information of text without causing real domain drift and bringing extra boundary priors.

methods in aligning with the real domain. As shown in Fig. 2(b), their highest score is only 78.9%. The observation implies that these domain-bridging methods may introduce intermediate domains and disrupt the real domain.

To conquer this domain drift issue, we propose FreeReal, a real-domain-aligned pre-training paradigm, leveraging synthetic labels to guide text detector learning on real-domain-aligned images. Specifically, a glyph-based mixing mechanism, named GlyphMix, is tailored for text images to create real-world images with annotations derived from synthetic labels. This involves delineating the glyphs of synthetic images based on their internal structure and embedding them as graffiti-like units onto any unlabeled real images. GlyphMix offers several advantages: 1) extracting glyph structures in a cost-effective way without introducing extra boundary priors; 2) leveraging synthetic labels for free while greatly minimizing real domain drift (achieving a confidence score of 95.7%).

As a byproduct, FreeReal can bridge the language-to-language gap illustrated in Fig. 3, when adapting features learned from English-dominated LSD to URD in various languages. Specifically, given free character-level synthetic labels, FreeReal enables the pre-trained model to easily learn character features, since characters are the underlying unit of any language. Subsequently, during fine-tuning, these learned character features are adaptively combined according to the rules (*e.g.*, word- and sentence-level) provided by available benchmarks.

Building upon these insights, we break the trend of recent pre-training methods for scene text detectors (PSTD) that combine increasingly complex pretext task designs or more training modules to improve performance. Without bells and whistles, we focus on exploring the potential of integrating the LSD and URD. Remarkably, despite using



Figure 3. We illustrate differences in character, word, and sentence spacing between LSD and URD. When leveraging their inherent properties to improve text detection, the divergence in spacing can confuse the pre-trained model, making it challenging to interpret text layout and semantic context. For example, the model predictions cover text areas well but yield low F-measure values in (c). Green areas are filled by ground-truths, while red polygons indicate network predictions.

90% less LSD than recent SOTAs, our method still attains a 1.2% gain, effectively underscoring the superiority of our pre-training paradigm. As shown in Table 1, FreeReal consistently surpasses recent SOTAs by a large margin. The main contributions are summarized as follows:

- We are the first to simultaneously integrate labeled synthetic data and unlabeled real data for enhancing the pre-training of text detectors. FreeReal shows its superiority and significant performance gains over other complex alternatives, serving as a simple yet strong baseline for future PSTD studies.
- We effectively address the challenges of synthetic-to-real and language-to-language domain adaptation. Without bringing boundary priors and causing real domain drift, we freely harness the strengths of real-world text images with annotations derived from synthetic labels.

2. Related Work

2.1. Scene Text Detection

Existing scene text detection methods delineate text regions by point-based or segmentation-based representations. The point-based methods [8, 13, 23, 44, 62] directly regress the bounding points to enclose text regions, and gradually increase the number of points as required to detect complex scenes, *e.g.*, arbitrary texts. The segmentation-based representations regard arbitrary-shape texts by grouping pixel-level [20, 21, 42], character-level [1, 9], segment-level [25, 33] or contour-level [39, 45] segmentation results by post-processing.

2.2. Pre-training for Scene Text Detector

In early research, [11, 19, 24] proposed to pre-train scene text detectors by generating synthetic data. These data engine tools follow the same paradigm: they first stack multiple off-the-shelf models to perform semantic segmentation and depth estimation analysis on background images, and then blend pre-processed texts into these images. However, the multi-stage, pre-generated methods incur large computational costs (GPU and CPU resources) and substantial latency, making them unsuitable for on-line training tasks where immediate data processing is essential. Inspired by recent advancements in pre-training techniques [4, 5, 10, 32], the integration of text and visual cross-modal information into scene text detectors has garnered increasing attention. One representative work involves enhancing the backbone with text transcriptions. For example, STKM [38] proposes a pioneering work that pre-trains the backbone through an image-level text recognition task. VLPT [35] formulates three cross-modality pretext tasks to boost better text representations derived from the backbone. Another representative work is to endow the entire detector with pre-trained vision-text knowledge. Inherited from CLIP [32], TCM incorporates the Image and Text encoders into the text detector to refine text regions using cross-modal visual-language priors. A persistent challenge still remains—the synth-to-real domain gap limits the detection performance.

2.3. Semi-Supervised Learning

Due to the scarcity of expensive and labor-intensive annotations, semi-supervised learning (SSL) methods are becoming increasingly important. These methods extract knowledge from a reduced amount of annotated images in a supervised manner, and from a larger amount of unlabeled images in an unsupervised way. In scenarios where both labeled and unlabeled data are from the same domain, the challenge involves leveraging the intrinsic qualities of the unlabeled data to improve model performance. In scenarios where labeled and unlabeled data belong to different domains, the challenge involves adapting a model trained on

labeled data from a source domain to perform well on unlabeled data from a target domain. This situation is called unsupervised domain adaptation. Commonly, a self-training framework for SSL is employed, which encourages a model (student) to learn unlabeled images from pseudo-labels generated by the up-to-date optimized model (teacher). To avoid overfitting incorrect pseudo-labels, recent advancements have focused on pseudo-label refinement by improving the reliability [34, 58] and pseudo-label regularization by cross-view consistency [18, 37, 46].

3. Methodology

Problem setting: Given a labeled synthetic set $\mathcal{D}_l = \{(\mathbf{X}_l^{(i)}, \mathcal{B}_l^{(i)})\}_{i=1}^{N_l}$ with N_l samples, $\mathbf{X}_l^{(i)} \in \mathbb{R}^{H \times W \times 3}$ represents an image and $\mathcal{B}_l^{(i)} = \{(p_{lt}^i, p_{lb}^i, p_{rt}^i, p_{rb}^i)\}_{i=1}^n$ is its corresponding set of bounding boxes. p refers to the values of the vertice along the abscissa and ordinate, and n denotes the number of bounding boxes. H and W are the height and width of the image. Similarly, the unlabeled real set is denoted as $\mathcal{D}_u = \{\mathbf{X}_u^{(i)}\}_{i=1}^{N_u}$ with N_u samples. Our objective is to jointly leverage labeled synthetic data \mathcal{D}_l and unlabeled real data \mathcal{D}_u by bridging their gap for enhancing the pre-training of scene text detectors.

3.1. Overview

The student-teacher framework exhibits substantial efficacy due to its dual capacity for knowledge transfer between its two branches, which is typically employed to mitigate the domain gap (*e.g.*, data and multimodal). Accordingly, we customize it for aligning real and synthetic text data, as illustrated in Fig. 4. For notation simplification in the following introduction, we omit the superscript i as mentioned above.

Specifically, the segmentation-based text detector DB-Net [20] is employed as our baseline model, primarily due to its impressive real-time performance, versatility, and practical applicability. In the teacher branch, the teacher model parameterized by \mathbf{f}_t , is responsible for generating truncated-gradient logits $\hat{\mathbf{Y}}_u \in \mathbb{R}^{H \times W}$ from a weakly augmented unlabeled real image $w(\mathbf{X}_u)$. The pseudo label $\mathbf{Y}_u \in \{0, 1\}^{H \times W}$ is then obtained by binarizing the logit map $\hat{\mathbf{Y}}_u$. In the student branch, the process begins by generating a pixel-wise binary map $\mathbf{Y}_l \in \{0, 1\}^{H \times W}$, where 1 is assigned to locations within all bounding boxes from annotation \mathcal{B}_l , and 0 otherwise. The labeled synthetic image \mathbf{X}_l and the strongly augmented unlabeled real image $s(\mathbf{X}_u)$ are combined to create $\mathbf{X}_g = \mathbb{A}(s(\mathbf{X}_u), \mathbf{X}_l)$, with $\mathbb{A}(\cdot)$ denoting our proposed GlyphMix mechanism, which will be introduced later. Subsequently, the mixed image \mathbf{X}_g serves as input to train the student model, under the supervision of mixed pseudo-labels $\mathbf{Y}_g = \mathbb{A}(\mathbf{Y}_u, \mathbf{Y}_l)$, by minimizing loss

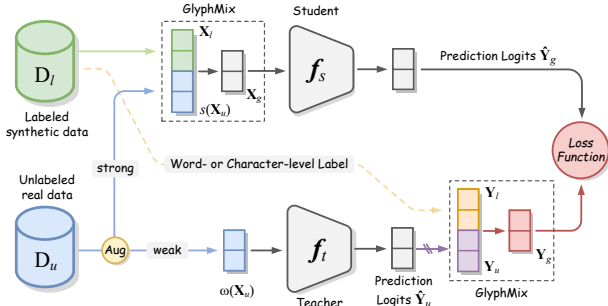


Figure 4. Our network pipeline in a student-teacher framework.

in the following:

$$\mathcal{L} = \ell_{DB}(\hat{\mathbf{Y}}_g, \mathbf{Y}_g, \mathbf{E}), \quad (1)$$

where ℓ_{DB} denotes the original loss function provided by DBNet [20] and $\hat{\mathbf{Y}}_g$ represents the prediction logits generated by the student model. The matrix $\mathbf{E} \in \mathbb{R}^{H \times W}$, which indicates positive regions for loss calculation, is set as an all-one matrix by default.

To filter out the unreliable predictions in mixed pseudo-labels \mathbf{Y}_g , we adaptively adjust the matrix \mathbf{E} during pre-training. Specifically, for the labeled synthetic image \mathbf{X}_l , the positive regions \mathbf{E}_l are an all-one matrix. For the unlabeled real image \mathbf{X}_u , we compute the pixel-wise entropy map on $\hat{\mathbf{Y}}_u$ and then apply a dynamic entropy threshold ζ to obtain its positive regions \mathbf{E}_u as follows:

$$\mathbf{E}_u = \mathbb{I}(-\hat{\mathbf{Y}}_u \log \hat{\mathbf{Y}}_u \leq \zeta), \quad (2)$$

where $\mathbb{I}(\cdot)$ denotes the indicator function. The matrix is subsequently formulated as $\mathbf{E} = \mathbf{A}(\mathbf{E}_u, \mathbf{E}_l)$. In our experiments, the threshold ζ is determined by the value corresponding to the top γ percent of the entropy map. As the reliability of pseudo-label gradually improves, we smoothly update γ using `np.linspace(80, 20, t)`, where t denotes the total number of training iterations.

Finally, the teacher model f_t gradually updates itself via the exponential moving averaging (EMA) of the student weights f_s as follows:

$$\mathbf{f}_t = \alpha \mathbf{f}_t + (1 - \alpha) \mathbf{f}_s, \quad (3)$$

where α is a momentum parameter, set as 0.996 by default.

3.2. GlyphMix

Although some efforts [30, 57, 60] attempt to aggregate the advantages of synthetic and unlabeled images through versatile transformations, they inevitably introduce intermediate domains, leading to real domain drift. In this section, we present a domain-bridging way tailored for text images, allowing for the free use of synthetic labels while ensuring consistent alignment with the real domain.

1) Graffiti-like Inter-domain Mixing. Given an input synthetic image \mathbf{X}_l , its corresponding bounding box annotations \mathcal{B}_l and converted pixel-wise binary map \mathbf{Y}_l , our goal is to perform character segmentation. This process iden-

tifies all character structure regions and produces a mask \mathbf{M}_G .

To achieve this, we begin with an unsupervised clustering task based on the grayscale values of pixels, avoiding the introduction of extra pixel-level annotation costs. This involves aligning and cropping the image according to the coordinates of each bounding box, yielding a set of image patches $\mathcal{T} = \{\mathbf{T}^{(i)} | \mathbf{T}^{(i)} \in \mathbb{R}^{w_i \times h_i \times 3}\}_{i=1}^n$. Subsequently, within each image patch $\mathbf{T}^{(i)}$, we cluster the pixels into two regions: the glyph region representing character structures and the background region. For simplicity, we focus our study on K-means to implement the clustering task, but other clustering approaches with predefined categories can be used. Following this, the glyph regions from all image patches are pasted to an all-zero image to create the character structure mask \mathbf{M}_G .

Given the pseudo label \mathbf{Y}_u produced by the teacher model on an unlabeled real image \mathbf{X}_u , we use \mathbf{M}_G to generate the inter-domain mixing image and its corresponding label. This process can be formulated as follows:

$$\begin{cases} \mathbf{A}^G(\mathbf{X}_u, \mathbf{X}_l) \leftarrow \mathbf{M}_G \odot \mathbf{X}_l + (\mathbf{1} - \mathbf{M}_G) \odot \mathbf{X}_u, \\ \mathbf{A}^G(\mathbf{Y}_u, \mathbf{Y}_l) \leftarrow \mathbf{M}_G \odot \mathbf{Y}_l + (\mathbf{1} - \mathbf{M}_G) \odot \mathbf{Y}_u, \end{cases} \quad (4)$$

where $\mathbf{1}$ is an all-one matrix and \odot denotes the element-wise multiplication operation. \mathbf{M}_G indicates pixels occupied by the glyph need to be copied from the synth domain and pasted to the real domain. Thus the mixed image closely aligns with the real domain, taking advantage of the freely available synthetic labels. Put simply, this process produces real-world images with annotations.

2) Text-balanced Intra-domain Mixing. Real-world text images inherently exhibit complexity, and the collected unlabeled data often struggles to comprehensively represent the full spectrum of real-world scenarios. Within a student-teacher framework, intra-domain mixing serves as an effective perturbation technique, enriching the diversity of real data and enhancing feature consistency and robustness. However, when randomly generating and applying binary masks to construct intra-domain mixing images and their corresponding labels, there is a risk of missing many text regions, especially considering that text regions typically occupy only a small fraction of an image. To mitigate this challenge, our objective is to retain more text regions while still maintaining randomness.

In light of this, we initiate the process by randomly selecting two unlabeled real images, denoted as $(\mathbf{X}_u^{(1)}, \mathbf{X}_u^{(2)})$, and obtaining the corresponding segmentation pseudo-labels, $(\mathbf{Y}_u^{(1)}, \mathbf{Y}_u^{(2)})$, produced by the teacher model. Subsequently, k rectangular boxes $\{(p_{lt}^i, p_{lb}^i, p_{rt}^i, p_{rb}^i)\}_{i=1}^k$ are randomly generated to crop the pseudo-label $\mathbf{Y}_u^{(2)}$ based on their coordinates. This operation yields a set of local pseudo-label regions $\mathcal{S} = \{\mathbf{S}^{(i)} | \mathbf{S}^{(i)} \in \mathbb{R}^{w_i \times h_i}\}_{i=1}^k$. Following this, we identify the rectangular

box that contains the maximum text regions by calculating $\arg \max_i \sum_{j=1}^{w_i \times h_i} \mathbf{S}_j^{(i)}$, and convert it into a binary mask, denoted as \mathbf{M}_T . Finally, we employ \mathbf{M}_T to generate the intra-domain mixed image and its corresponding label, following the formulated procedure:

$$\begin{cases} \mathbb{A}^T(\mathbf{X}_u) \leftarrow \mathbf{M}_T \odot \mathbf{X}_u^{(2)} + (\mathbf{1} - \mathbf{M}_T) \odot \mathbf{X}_u^{(1)}, \\ \mathbb{A}^T(\mathbf{Y}_u) \leftarrow \mathbf{M}_T \odot \mathbf{Y}_u^{(2)} + (\mathbf{1} - \mathbf{M}_T) \odot \mathbf{Y}_u^{(1)}, \end{cases} \quad (5)$$

where $\mathbf{1}$ is an all-one matrix and \odot represents the element-wise multiplication.

3) **Intra- and Inter-domain Mixing.** When these two strategies, tailored for scene text images, are integrated within the student-teacher framework, they collectively form a comprehensive method that effectively harnesses the strengths of both synthetic and real data. The whole process can be formulated as:

$$\begin{cases} \mathbb{A}(\mathbf{X}) \leftarrow \mathbb{A}^G(\mathbb{A}^T(\mathbf{X}_u), \mathbf{X}_l), \\ \mathbb{A}(\mathbf{Y}) \leftarrow \mathbb{A}^G(\mathbb{A}^T(\mathbf{Y}_u), \mathbf{Y}_l) \end{cases} \quad (6)$$

Consequently, the synergy maximizes the utilization of synthetic labels as a valuable resource, effectively tackling the intricacies of real-world scenarios.

3.3. Discussion on Character Region Awareness

As illustrated in Fig. 3, existing LSD only contains English texts with tightly spaced characters, while URD may encompass text properties from various languages (such as Japanese, Korean, Chinese, *etc.*). Consequently, even though the model predictions effectively cover text regions, we encounter challenges in parsing these predictions into word-level bounding boxes or polygons.

Indeed, when using a single language (*e.g.*, English) as the source domain and adapting it to various language domains, it appears that no matter how sophisticated the models and loss functions are, they struggle to accurately and effectively parse the complex text layout and semantic context. This challenge primarily arises from variations in the spacing and arrangement of characters, words, and sentences across languages. This observation leads us to revisit the learning objective of scene text detectors during pre-training.

We emphasize an alternative perspective – utilizing characters as the fundamental learning unit for text detection. The strategy presents several advantages: 1) Like word-level bounding boxes (WBB), character-level bounding box (CBB) annotations can be readily acquired from the existing synthetic dataset (SynthText) at no additional cost; 2) Instead of parsing complex layouts and spacing disparities across languages during pre-training, decoding them into individual characters is straightforward and attainable; 3) The pre-trained model with character-level region awareness easily integrates its learned character features to adapt text attribute rules provided by different language text datasets during fine-tuning. To this end, we se-

lect CBB annotations as \mathcal{B}_l . Following the pipeline outlined in Fig. 4, the mixed image \mathbf{X}_g is created by cropping the synthetic image \mathbf{X}_l using CBB annotations \mathcal{B}_l and pasting its glyphs onto the unlabeled image \mathbf{X}_u . The corresponding mixed pseudo labels \mathbf{Y}_g are then obtained by combining the pixel-wise binary map \mathbf{Y}_l which is converted from \mathcal{B}_l , with the estimated character-level pseudos \mathbf{Y}_u generated by the teacher branch.

4. Experiment

4.1. Dataset

Labeled Synthetic Data (LSD). The SynthText [11] serves as our source of LSD, consisting of 800K images. Each image is provided with character-level and word-level bounding boxes, along with corresponding text transcriptions.

Unlabeled Real Data (URD). Our collected URD is sourced from a wide array of natural scenes, encompassing a diverse range of fonts, languages, text shapes, and sizes. Specifically, URD includes 430K images from LSVT [36], 9K from MLT17 [27], 19657 from MLT19 [28], 229 from IC-DAR2013 [16], and 500 from USTB-SV1K [54].

Benchmarks. Our method is designed to detect text with arbitrary shapes, including oriented and curved texts from the following publicly available benchmarks:

Total-Text (TT) [6] consists of 1255 training images and 300 test images. It contains many curved text instances with polygon-shaped bounding box annotations.

CTW 1500 (CTW) [22] mainly focuses on curved texts and consists of 1000 training images and 500 test images with polygon-shaped bounding box annotations.

ICDAR2015 (IC15) [17] contains 1000 training images and 500 testing images with word-level rectangular bounding box annotations.

MSRA-TD500 (TD) [50] includes 300 training images and 200 test images with line-level rectangular bounding box annotations. HUST-TR400 dataset [51] is typically added to train the model.

4.2. Implementation Details

Referring to recent works [35, 38, 48], we combine representative text detection methods [20, 41, 42, 62] to conduct experiments. All experiments are implemented on a server with 2 NVIDIA A800 GPUs, using PyTorch.

1) Pre-Training. The pre-training experiments are conducted on LSD and URD, utilizing the open-source codes provided by these text detection methods. For synthetic images, we adopt consistent augmentation settings as prescribed by these methods for a fair comparison. For unlabeled real images, we employ a standard weak-to-strong augmentation technique [61] to enrich diversity. Our method is trained using the AdamW optimizer [26], along with a cosine learning rate scheduler [7]. This includes a

Table 1. Comparison with SOTA pre-training methods for text detectors on TT, CTW, IC15, and TD. F-measure (%) is reported. * denotes the use of extra labeled real data. For easy reference, we mark these symbols †, *, ‡, and * separately to indicate the results from [56], [35], [48], and [40], within the scope of this paper. The best results are shown in **bold font**. The second-best results are underlined.

Index	Method	Venue	TT	CTW	IC15	TD
1	PSENet-1s [41]	CVPR'19	80.9	82.2	85.7	-
	LOMO [59]	CVPR'19	81.6	78.4	87.2	-
	MOST [13]	CVPR'21	-	-	88.2	86.4
	PAN++ [43]	PAMI'21	85.3	84.0	84.5	87.9
	DBNet++ [21]	PAMI'22	86.0	85.3	87.3	87.2
	DeepSOLO* [53]	CVPR'23	87.6	-	89.8	-
	ESTextSpotter* [14]	ICCV'23	90.0	-	91.0	89.5
	SIR [31]	ACM MM'23	88.2	85.5	87.8	89.6
2	DBNet+ST† [20]	AAAI'20	84.7	83.4	85.4	84.9
	DBNet+STKM† [38]	CVPR'21	85.5	-	86.1	85.9
	DBNet+VLPT† [35]	CVPR'22	<u>86.3</u>	-	86.5	88.5
	DBNet+oCLIP† [48]	ECCV'22	84.1	82.0	85.4	-
	DBNet+TCM† [55]	CVPR'23	85.9	<u>85.1</u>	<u>89.4</u>	<u>88.8</u>
	DBNet+MTM* [40]	ACM MM'23	85.7	-	-	85.6
	DBNet+FreeReal (ours)	-	88.9 _(+2.6)	87.9 _(+2.8)	90.0 _(+0.6)	90.1 _(+1.3)
3	PANet+ST† [42]	ICCV'19	<u>85.0</u>	83.7	82.9	84.1
	PANet+TCM† [55]	CVPR'23	-	<u>84.3</u>	<u>84.6</u>	<u>85.3</u>
	PANet+FreeReal (ours)	-	87.4 _(+2.4)	88.4 _(+4.1)	86.0 _(+1.4)	89.9 _(+4.6)
4	PSENet+ST* [41]	CVPR'19	83.9	81.6	81.3	-
	PSENet+STKM* [38]	CVPR'21	84.3	82.9	83.7	-
	PSENet+VLPT* [35]	CVPR'22	<u>86.1</u>	<u>83.3</u>	<u>84.3</u>	-
	PSENet+oCLIP† [48]	ECCV'22	85.5	82.8	-	-
	PSENet+FreeReal (ours)	-	86.8 _(+0.7)	86.1 _(+2.8)	85.2 _(+0.9)	86.0
5	FCENet+ST† [62]	CVPR'21	<u>85.8</u>	85.5	86.2	85.4
	FCENet+oCLIP† [48]	ECCV'22	-	85.6	86.7	-
	FCENet+TCM† [55]	CVPR'23	-	<u>85.9</u>	<u>87.1</u>	<u>86.9</u>
	FCENet+FreeReal (ours)	-	87.9 _(+2.1)	87.2 _(+1.3)	87.7 _(+0.6)	89.0 _(+2.1)

warm-up phrase for 1 epoch in a total of 10 epochs. The base learning rate is set to $0.003 \times \text{batchsize}/256$. At each iteration, we equally sample LSD and URD with a total batch size of 24.

2) Fine-Tuning. For a fair comparison, we employ the same fine-tuning configurations as these detection methods and then evaluate them on these publicly available benchmarks: TT, CTW, IC15 and TD, following the standard metric: Precision (P), Recall (R), and F-measure (F).

4.3. Experiment Results

To ensure a comprehensive comparison, we collect results from public evaluation benchmarks reported by existing pre-training methods, and organize them in Table 1. The sources of these results are clearly recorded in the table’s caption using different symbols for easy reference. Specifically, these methods can be classified into three pre-training paradigms. In Paradigm A, models (*i.e.*, +*ST*, +*TCM*) are initially pre-trained on LSD and then fine-tuned on real datasets directly. In Paradigm B, models (*i.e.*, +*STKM*, +*VLPT*, +*oCLIP*) are first pre-trained on LSD by various pretext tasks, and the well-learned backbone weights are transferred into scene text detectors when fine-tuning on real datasets. In Paradigm C, models (*i.e.*, +*MTM*) are pre-trained on URD by pretext tasks and on LSD by supervised learning, and then fine-tuned on real datasets.

1) Results on DBNet. As indicated in the second group of

rows in Table 1, all pre-training methods both report their cooperative performance with DBNet. When compared to methods using paradigm A, differing from *DBNet+ST*, we exclude the use of a deformable convolutional network (DCN) in our model. Despite these differences, our method still achieves impressive results, yielding improvements of 4.2%, 4.5%, 4.6%, and 5.2% on TT, CTW, IC15, and TD datasets, respectively. Compared to *DBNet+TCM* methods, our method achieves SOTA detection performance on four datasets, particularly on curved text datasets (TT and CTW), with gains of 3.0% and 2.8%, respectively. In comparison with methods following Paradigm B, our method consistently outperforms previous SOTA works by substantial margins, achieving performance improvements of 2.6%, 5.9%, 3.5% and 1.6% on TT, CTW, IC15, and TD datasets, respectively. In comparison with *DBNet+MTM* following Paradigm C, our method gets 3.2% and 4.5% gains on TT and TD datasets, respectively.

2) Results on PANet. As shown in the third group of rows in Table 1, our method outperforms *PANet+ST* on four benchmarks, achieving a gain of 3.85% in terms of average F-measure, while using the same parameters and labeled data for pre-training and fine-tuning. Furthermore, our method exhibits its prominent superiority, particularly on the CTW and TD datasets, surpassing the *PANet+TCM* method by a substantial margin of 4.1% and 4.6%, respectively.

Table 2. Comparison with existing pre-training paradigms when fine-tuning on the TotalText dataset. These symbols †, ‡, and * indicate the results from [56], [48] and [40], respectively. ΔF is the improvement relative to the baseline.

Paradigm	Method	Venue	Data		F-measure	$\Delta F(\%)$
			LSD	URD		
-	DBNet† [20]	AAAI'20	-	-	78.2	-
A	DBNet+ST† [20]	AAAI'20	800K	-	84.7	+6.5%
	DBNet+TCM† [55]	CVPR'23	800K	-	85.9	+7.7%
B	DBNet+STKM† [38]	CVPR'21	800K	-	85.5	+7.3%
	DBNet+VLPT† [35]	CVPR'22	800K	-	86.3	+8.1%
	DBNet+oCLIP‡ [48]	ECCV'22	800K	-	84.1	+5.9%
C	DBNet+MTM* [40]	ACM MM'23	800K	41K	85.7	+7.5%
D	Ours (9%)	-	71K	41K	87.4	+9.2%
	Ours (10%)	-	80K	46K	87.5	+9.3%
	Ours (20%)	-	160K	92K	88.1	+9.9%
	Ours (50%)	-	400K	230K	88.3	+10.1%
	Ours (100%)	-	800K	460K	88.9	+10.7%

3) Results on PSENet. Based on the observation from the fourth group of rows from Table 1, only methods using paradigm B report the performance in collaboration with PSENet. In comparison to these methods, FreeReal brings 0.7%, 2.8%, and 0.9% gains on TT, CTW, and IC15 datasets, respectively.

4) Results on FCENet. In the last group of rows from Table 1, we conduct a comparative experiment with pre-training methods in collaboration with FCENet. It can be observed that FreeReal further refreshes the best text detection results and improves 2.1%, 1.3%, 0.6% and 2.1% on TT, CTW, IC15, and TD datasets, respectively. These experimental results demonstrate the robustness of FreeReal, even when cooperated with regression-based methods.

5) Paradigm Comparison. In this section, we aim to investigate which kinds of pre-training paradigms for text detectors are important and meaningful for future studies. To this end, we conduct a comparative analysis with three mainstream pre-training paradigms mentioned above, as summarized in Table 2. When compared to these well-curated designs at the cost of introducing additional auxiliary pretext tasks or more training modules, our proposed paradigm achieves a significant improvement of 1.2% (87.5 vs. 86.3), despite utilizing 10% of the labeled synthetic data and 10% of the unlabeled real data. This outcome underscores our ability to harness the potential of unlabeled real images. Moreover, when we gradually increase the proportion of the total training data, the text detection performance continues to improve. Specifically, our method achieves gains of 1.8%, 2.0%, and 2.6% at data fractions of 20%, 50%, and 100%, respectively, compared to the recent SOTA method. This outcome fully demonstrates the superiority of our pre-training paradigm, which jointly leverage LSD and URD by bridging their gap for enhancing the text detector pre-training.

6) Extensibility to DETR-based methods. We also incorporate DPText to conduct comparisons with supervised SOTA works using DETR-based networks, as summarized

Table 3. Comparison with DETR-based methods on TT and CTW datasets.

Method	Venue	TT	CTW	Para.
DPText [52]	AAAI'23	89.0	88.8	46M
SRFormer [3]	AAAI'24	90.0	89.6	51M
DPText+FreeReal (ours)	-	90.9	90.2	46M

Table 4. Comparison with supervised SOTA work on unseen language text. ‘‘R50’’ and ‘‘DeT’’ denote a ResNet50 and Deformable Transformer structure, respectively. * denotes the use of extra labeled real data.

Method	Venue	Backbone	Para.	FPS	F
ESTextSpotter*	ICCV'23	R50+DeT	56M	3.4	89.6
DBNet+FreeReal (ours)	-	R50	25M	11	90.3

Table 5. Evaluate the effectiveness of the proposed modules. ΔF is the improvement of F-measure relative to baseline. ‘‘Stu-Tea’’, ‘‘CRA’’, ‘‘GlyphMix’’ denote the standard student-to-teacher framework, using character-level bounding boxes (CBB), and the glyph-based mixing mechanism, respectively.

Stu-Tea	CRA	GlyphMix	$\Delta F(\%)$	P	R	F
×	×	×	-	87.1	82.5	84.7
✓	×	×	+1.31%	88.80	83.39	86.01
✓	✓	×	+1.73%	87.76	85.15	86.43
✓	×	✓	+3.12%	89.10	86.58	87.82
✓	✓	✓	+3.40%	88.81	87.40	88.10

in Table 3.

7) Results on Unseen Language Text. Our pre-trained model is capable of learning the basic character feature representations of languages and then combining them during fine-tuning. To show its robustness, we choose to evaluate on unseen language text dataset VinText [29]. FreeReal achieves an improvement of 0.7%, as shown in Table 4.

5. Ablations and analysis

Unless otherwise stated, all ablation experiments are implemented in collaboration with DBNet method [20] using 20% of LSD and 20% of URD and evaluated on the curved

Table 6. Evaluate the effectiveness of GlyphMix components. “GIM” and “TIM” denote the Graffiti-like Inter-domain Mixing and Text-balanced Intra-domain Mixing.

GIM	TIM	$\Delta F(\%)$	P	R	F
×	×	-	87.76	85.15	86.43
×	✓	+1.22%	88.64	86.68	87.65
✓	×	+1.28%	88.29	87.13	87.71

TotalText (TT) dataset for efficiency.

Effectiveness of Network Components. To comprehensively evaluate the effectiveness of our proposed method, we divide it into three components and evaluate each one individually, as shown in Table 5. “Stu-Tea”, “CRA”, “GlyphMix” denote the standard student-to-teacher framework, Character Region Awareness introduced in Sec.3.3 to bridge the linguistic domain gap, and the glyph-based mixing mechanism, respectively. First, we enhance the baseline DBNet model by incorporating a standard student-teacher framework, yielding a performance gain of 1.31%. Second, within the student-teacher framework, we evaluate the individual contributions of the CRA and GlyphMix components, achieving 1.73% and 3.12% performance improvements, respectively. Finally, upon combining all plug-ins, the overall performance reaches 88.1%, showing a substantial gain of 3.40% compared to the baseline. These experiments consistently demonstrate that FreeReal effectively bridges both the synth-to-real and language-to-language domain gaps when leveraging the intrinsic qualities of unlabeled real data.

Discussion on Using WBB or CBB. The SynthText dataset offers word-level and character-level annotations, with the latter being exploited in our method to bridge the linguistic domain gap, bringing a 0.4% gain as shown in the third row of Table 5. Notably, even without the use of CRA, our method still achieves an F-measure of 87.82% (in the fourth row), significantly surpassing recent SOTAs.

Effectiveness of GlyphMix Components. In Table 6, GlyphMix comprises two modules, inter-domain GIM and intra-domain TIM, contributing gains of 1.28% and 1.22% to the final performance, respectively. Besides, when compared to the data engine tool [11], GIM achieves intra-domain mixing in a cost-effective way, which yields real-world images online via K-means, a more flexible, faster and direct process than the multi-stage, pre-generated method. Specifically, GIM attains a 10.7x speedup (2.6h vs 27.7h) in generating 92K images, which is more suitable for real-time online training tasks. Additionally, GIM can avoid improper text blends on URD by leveraging the learned knowledge (boxes/maps) from our pre-training framework online. We also conduct the ablations and get 0.5% (85.3% vs 84.8%) performance gains, when using 5% training data.

Comparison with pre-training methods using URD. Enabling the complementary strengths of both LSD and URD

Table 7. Comparison of the effectiveness with existing domain bridging methods. “DCA” refers to Domain Classification Accuracy in aligning with the real domain.

method	DCA	P	R	F	$\Delta F(\%)$
Stu-Tea	-	88.80	83.39	86.01	-
Mixup[60]	69.5	89.17	84.12	86.57	+0.56%
CutMix[57]	72.8	87.99	85.64	86.80	+0.79%
ClassMix[30]	78.9	90.65	83.61	86.99	+0.98%
FreeReal (ours)	95.7	88.81	87.40	88.10	+2.09%

is one of our contributions, a capability not present in other pre-training methods. Thus we conduct the experiments using URD to show the significant superiority in the pre-training paradigm and performance, as shown in Table 1-4. Besides, we add the comparison: using URD to train other pre-training methods. A possible way is to adopt self-supervised learning since there are no text labels for images in URD. In this case, these mentioned methods can be viewed the same as MTM [40]. As a result, FreeReal outperforms MTM by 1.7%, as presented in Table 2.

Comparison with Bridging-domain Methods. In this section, we begin with a domain classification experiment, calculating the confidence that the mixed images generated by domain bridging methods belong to the real domain. To accomplish this, we employ a network architecture, consisting of resnet18 as a feature extractor, followed by a binary classification head, for simplicity. The primary objective is to distinguish between synthetic and real images by assigning them to different classes. Subsequently, we employ the well-established network to evaluate the performance of different domain bridging methods, as summarized in Table 7. Remarkably, when compared to these methods, GlyphMix achieves an outstanding performance score of 95.7%, surpassing the second-best method by a substantial margin of 16.8%. This result demonstrates that our method is able to generate arbitrarily realistic images without domain drift.

To be more convincing, we also conduct text detection experiments to assess the effectiveness. As depicted in Table 7, our method consistently outperforms others, achieving the best F-measure value. Furthermore, the observed positive correlation between DCA and F-measure reinforces the idea that bridging the domain gap is the crucial factor in improving text detection performance.

Comparison with Semi-supervised Methods. In this section, we compared the performance with recent SSL methods. These methods tend to adopt increasingly complex designs, involving advanced contrastive learning techniques, additional network components, multiple ensemble models, and complex training procedures. However, some designs, such as Gentle Teaching Assistant, may not be conducive to text feature learning because they do not fully consider the noticeable domain gap in text images. In contrast, we aim to eliminate domain gaps between LSD and URD. De-

Table 8. Comparison of the effectiveness with SSL methods.

Method	Venue	P	R	F	$\Delta F(\%)$
Stu-Tea	-	88.80	83.39	86.01	-
GTA[15]	NeurIPS'22	87.18	81.08	84.02	-1.99%
BCP[2]	CVPR'23	86.72	85.82	86.27	+0.26%
AugSeg[61]	CVPR'23	88.48	85.65	87.04	+1.03%
Unimatch[49]	CVPR'23	88.94	85.56	87.22	+1.21%
FreeReal (ours)	-	88.81	87.40	88.10	+2.09%

spite adopting the standard student-teacher framework, our method still exceeds the previous SOTA by 0.88% in Table 8.

Effectiveness of M_G . We evaluate the accuracy of character segmentation results M_G using TotalText [6] and TextSeg [47] datasets, both of which provide pixel-level annotations. Specifically, compared to conducting the cluster task on the whole image, we crop it into several text instances and then perform clustering to form M_G . While the accuracy of the former is 32.35% for TotalText and 45.54% for TextSeg, M_G achieves 80.43% and 84.14%, respectively. Notably, the underlying morphological representations of glyphs exhibit relative invariance to slight structural changes, such as thicker or thinner. This reduces the dependence on pixel-level high-precision segmentation with expensive costs. Furthermore, although the clustering process introduces some noise, leading to inaccuracies in M_G , it can still be viewed as a way of adding data noise in the image-mixing process, enhancing the robustness of text detection.

Ablation Study on Hyper-parameters. We study the impact of the parameter γ on the pseudos generated by the teacher model during pre-training. This parameter controls the proportion of unreliable and reliable pixels. With γ set at 80, 50, and 20, the F-measure are 87.94%, 87.68%, and 87.06%, respectively. Finally, we employ a linear warm-up strategy for γ that gradually reduces from 80 to 20, yielding the best result with an F-measure of 88.10%.

6. Conclusion

We propose an effective pre-training paradigm for scene text detection, situated within a standard student-teacher framework. The paradigm leverages the complementary strengths of both labeled synthetic data (LSD) and unlabeled real data (URD), standing out from existing intricate pre-training paradigms in text detection due to its simplicity and significant advancements. Moreover, we identify and address prominent challenges, *i.e.*, synth-to-real and language-to-language domain gaps. The proposed solutions, namely GlyphMix and character region awareness, have shown their effectiveness in mitigating these challenges and improving text detection performance, as substantiated by extensive experimental results. More importantly, our method exhibits the ability to harness the intrinsic

attributes of URD, achieving substantial performance improvements even with a small fraction of LSD. This highlights the significance of exploring the potential of unlabeled real data in scene text detection, ultimately advancing the field and its practical applications.

References

- [1] Youngmin Baek, Bado Lee, Dongyoon Han, Sangdoon Yun, and Hwalsuk Lee. Character region awareness for text detection. In *CVPR*, pages 9365–9374, 2019. 3
- [2] Yunhao Bai, Duowen Chen, Qingli Li, Wei Shen, and Yan Wang. Bidirectional copy-paste for semi-supervised medical image segmentation. In *CVPR*, pages 11514–11524, 2023. 9
- [3] Qingwen Bu, Sungrae Park, Minsoo Khang, and Yichuan Cheng. Srformer: Empowering regression-based text detection transformer with segmentation. *arXiv:2308.10531*, 2023. 7
- [4] Mathilde Caron, Hugo Touvron, Ishan Misra, Hervé Jégou, Julien Mairal, Piotr Bojanowski, and Armand Joulin. Emerging properties in self-supervised vision transformers. In *ICCV*, pages 9650–9660, 2021. 3
- [5] Ting Chen, Simon Kornblith, Mohammad Norouzi, and Geoffrey Hinton. A simple framework for contrastive learning of visual representations. In *ICML*, pages 1597–1607, 2020. 3
- [6] Chee-Kheng Ch'ng, Chee Seng Chan, and Cheng-Lin Liu. Total-text: toward orientation robustness in scene text detection. *IJDAR*, 23(1):31–52, 2020. 5, 9
- [7] Jean-Bastien Grill, Florian Strub, Florent Alché, et al. Bootstrap your own latent - A new approach to self-supervised learning. In *NeurIPS*, pages 21271–21284, 2020. 5
- [8] Tongkun Guan, Chaochen Gu, Changsheng Lu, Jingzheng Tu, Qi Feng, Kaijie Wu, and Xiping Guan. Industrial scene text detection with refined feature-attentive network. *IEEE TCSVT*, 32(9):6073–6085, 2022. 1, 3
- [9] Tongkun Guan, Chaochen Gu, Jingzheng Tu, Xue Yang, Qi Feng, Yudi Zhao, and Wei Shen. Self-supervised implicit glyph attention for text recognition. In *CVPR*, pages 15285–15294, 2023. 3
- [10] Tongkun Guan, Wei Shen, Xue Yang, Qi Feng, Zekun Jiang, and Xiaokang Yang. Self-supervised character-to-character distillation for text recognition. In *ICCV*, pages 19473–19484, 2023. 3
- [11] Ankush Gupta, Andrea Vedaldi, and Andrew Zisserman. Synthetic data for text localisation in natural images. In *CVPR*, pages 2315–2324, 2016. 3, 5, 8
- [12] Kaiming He, Xinlei Chen, Saining Xie, Yanghao Li, Piotr Dollár, and Ross Girshick. Masked autoencoders are scalable vision learners. In *CVPR*, pages 16000–16009, 2022. 1
- [13] Minghang He, Minghui Liao, Zhibo Yang, Humen Zhong, Jun Tang, Wenqing Cheng, Cong Yao, Yongpan Wang, and Xiang Bai. Most: A multi-oriented scene text detector with localization refinement. In *CVPR*, pages 8813–8822, 2021. 3, 6
- [14] Mingxin Huang, Jiabin Zhang, Dezhi Peng, Hao Lu, Can Huang, Yuliang Liu, Xiang Bai, and Lianwen Jin. Es-textspotter: Towards better scene text spotting with explicit

- synergy in transformer. In *ICCV*, pages 19495–19505, 2023. 6
- [15] Ying Jin, Jiaqi Wang, and Dahua Lin. Semi-supervised semantic segmentation via gentle teaching assistant. In *NeurIPS*, pages 2803–2816, 2022. 9
- [16] Dimosthenis Karatzas, Faisal Shafait, Seiichi Uchida, et al. Icdar 2013 robust reading competition. In *ICDAR*, pages 1484–1493, 2013. 5
- [17] Dimosthenis Karatzas, Lluís Gomez-Bigorda, Angelos Nicolaou, et al. Icdar 2015 competition on robust reading. In *ICDAR*, pages 1156–1160, 2015. 5
- [18] Samuli Laine and Timo Aila. Temporal ensembling for semi-supervised learning. *arXiv:1610.02242*, 2016. 3
- [19] Minghui Liao, Boyu Song, Shangbang Long, Minghang He, Cong Yao, and Xiang Bai. Synthtext3d: synthesizing scene text images from 3d virtual worlds. *Science China Information Sciences*, 63:1–14, 2020. 3
- [20] Minghui Liao, Zhaoyi Wan, Cong Yao, Kai Chen, and Xiang Bai. Real-time scene text detection with differentiable binarization. In *AAAI*, pages 11474–11481, 2020. 1, 3, 4, 5, 6, 7
- [21] Minghui Liao, Zhisheng Zou, Zhaoyi Wan, Cong Yao, and Xiang Bai. Real-time scene text detection with differentiable binarization and adaptive scale fusion. *IEEE TPAMI*, 45(1): 919–931, 2022. 3, 6
- [22] Yuliang Liu, Lianwen Jin, Shuaitao Zhang, Canjie Luo, and Sheng Zhang. Curved scene text detection via transverse and longitudinal sequence connection. *PR*, 90:337–345, 2019. 5
- [23] Yuliang Liu, Hao Chen, Chunhua Shen, Tong He, Lianwen Jin, and Liangwei Wang. Abcnet: Real-time scene text spotting with adaptive bezier-curve network. In *CVPR*, pages 9809–9818, 2020. 3
- [24] Shangbang Long and Cong Yao. Unrealtext: Synthesizing realistic scene text images from the unreal world. *arXiv:2003.10608*, 2020. 3
- [25] Shangbang Long, Jiaqiang Ruan, Wenjie Zhang, Xin He, Wenhao Wu, and Cong Yao. Textsnake: A flexible representation for detecting text of arbitrary shapes. In *ECCV*, pages 20–36, 2018. 3
- [26] Ilya Loshchilov and Frank Hutter. Decoupled weight decay regularization. *arXiv:1711.05101*, 2017. 5
- [27] Nibal Nayef, Fei Yin, Imen Bizid, et al. Icdar2017 robust reading challenge on multi-lingual scene text detection and script identification-rrc-mlt. In *ICDAR*, pages 1454–1459, 2017. 5
- [28] Nibal Nayef, Yash Patel, Michal Busta, et al. Icdar2019 robust reading challenge on multi-lingual scene text detection and recognition—rrc-mlt-2019. In *ICDAR*, pages 1582–1587, 2019. 5
- [29] Nguyen Nguyen, Thu Nguyen, Vinh Tran, et al. Dictionary-guided scene text recognition. In *CVPR*, pages 7383–7392, 2021. 7
- [30] Viktor Olsson, Wilhelm Tranheden, Juliano Pinto, and Lennart Svensson. Classmix: Segmentation-based data augmentation for semi-supervised learning. In *WACV*, pages 1369–1378, 2021. 1, 4, 8
- [31] Xugong Qin, Pengyuan Lyu, Chengquan Zhang, Yu Zhou, Kun Yao, Peng Zhang, Hailun Lin, and Weiping Wang. Towards robust real-time scene text detection: From semantic to instance representation learning. In *ACM MM*, pages 2025–2034, 2023. 6
- [32] Alec Radford, Jong Wook Kim, Chris Hallacy, et al. Learning transferable visual models from natural language supervision. In *ICML*, pages 8748–8763, 2021. 3
- [33] Baoguang Shi, Xiang Bai, and Serge Belongie. Detecting oriented text in natural images by linking segments. In *CVPR*, pages 2550–2558, 2017. 3
- [34] Kihyuk Sohn, David Berthelot, Nicholas Carlini, Zizhao Zhang, Han Zhang, Colin A Raffel, Ekin Dogus Cubuk, Alexey Kurakin, and Chun-Liang Li. Fixmatch: Simplifying semi-supervised learning with consistency and confidence. In *NeurIPS*, pages 596–608, 2020. 3
- [35] Sibong Song, Jianqiang Wan, Zhibo Yang, Jun Tang, Wenqing Cheng, Xiang Bai, and Cong Yao. Vision-language pre-training for boosting scene text detectors. In *CVPR*, pages 15681–15691, 2022. 1, 3, 5, 6, 7
- [36] Yipeng Sun, Zihan Ni, Chee-Kheng Chng, et al. Icdar 2019 competition on large-scale street view text with partial labeling-rrc-lsvt. In *ICDAR*, pages 1557–1562, 2019. 5
- [37] Antti Tarvainen and Harri Valpola. Mean teachers are better role models: Weight-averaged consistency targets improve semi-supervised deep learning results. In *NeurIPS*, 2017. 3
- [38] Qi Wan, Haoqin Ji, and Linlin Shen. Self-attention based text knowledge mining for text detection. In *CVPR*, pages 5983–5992, 2021. 1, 3, 5, 6, 7
- [39] Fangfang Wang, Yifeng Chen, Fei Wu, and Xi Li. Text-tray: Contour-based geometric modeling for arbitrary-shaped scene text detection. In *ACM MM*, pages 111–119, 2020. 3
- [40] Keran Wang, Hongtao Xie, Yuxin Wang, Dongming Zhang, Yadong Qu, Zuan Gao, and Yongdong Zhang. Masked text modeling: A self-supervised pre-training method for scene text detection. In *ACM MM*, pages 2006–2015, 2023. 1, 6, 7, 8
- [41] Wenhao Wang, Enze Xie, Xiang Li, Wenbo Hou, Tong Lu, Gang Yu, and Shuai Shao. Shape robust text detection with progressive scale expansion network. In *CVPR*, pages 9336–9345, 2019. 1, 5, 6
- [42] Wenhao Wang, Enze Xie, Xiaoge Song, Yuhang Zang, Wenjia Wang, Tong Lu, Gang Yu, and Chunhua Shen. Efficient and accurate arbitrary-shaped text detection with pixel aggregation network. In *ICCV*, pages 8440–8449, 2019. 3, 5, 6
- [43] Wenhao Wang, Enze Xie, Xiang Li, Xuebo Liu, Ding Liang, Zhibo Yang, Tong Lu, and Chunhua Shen. Pan++: Towards efficient and accurate end-to-end spotting of arbitrarily-shaped text. *IEEE TPAMI*, 44(9):5349–5367, 2022. 6
- [44] Xiaobing Wang, Yingying Jiang, Zhenbo Luo, Cheng-Lin Liu, Hyunsoo Choi, and Sungjin Kim. Arbitrary shape scene text detection with adaptive text region representation. In *CVPR*, pages 6449–6458, 2019. 3
- [45] Yuxin Wang, Hongtao Xie, Zheng-Jun Zha, Mengting Xing, Zilong Fu, and Yongdong Zhang. Contournet: Taking a fur-

- ther step toward accurate arbitrary-shaped scene text detection. In *CVPR*, pages 11753–11762, 2020. 1, 3
- [46] Haiming Xu, Lingqiao Liu, Qiuchen Bian, and Zhen Yang. Semi-supervised semantic segmentation with prototype-based consistency regularization. In *NeurIPS*, pages 26007–26020, 2022. 3
- [47] Xingqian Xu, Zhifei Zhang, Zhaowen Wang, Brian Price, Zhonghao Wang, and Humphrey Shi. Rethinking text segmentation: A novel dataset and a text-specific refinement approach. In *CVPR*, pages 12045–12055, 2021. 9
- [48] Chuhui Xue, Wenqing Zhang, Yu Hao, Shijian Lu, Philip HS Torr, and Song Bai. Language matters: A weakly supervised vision-language pre-training approach for scene text detection and spotting. In *ECCV*, pages 284–302. Springer, 2022. 1, 5, 6, 7
- [49] Lihe Yang, Lei Qi, Litong Feng, Wayne Zhang, and Yinghuan Shi. Revisiting weak-to-strong consistency in semi-supervised semantic segmentation. In *CVPR*, pages 7236–7246, 2023. 9
- [50] Cong Yao, Xiang Bai, Wenyu Liu, Yi Ma, and Zhuowen Tu. Detecting texts of arbitrary orientations in natural images. In *CVPR*, pages 1083–1090, 2012. 5
- [51] Cong Yao, Xiang Bai, and Wenyu Liu. A unified framework for multioriented text detection and recognition. *IEEE TIP*, 23(11):4737–4749, 2014. 5
- [52] Maoyuan Ye, Jing Zhang, Shanshan Zhao, Juhua Liu, Bo Du, and Dacheng Tao. Dptext-detr: Towards better scene text detection with dynamic points in transformer. In *AAAI*, pages 3241–3249, 2023. 7
- [53] Maoyuan Ye, Jing Zhang, Shanshan Zhao, Juhua Liu, Tongliang Liu, Bo Du, and Dacheng Tao. DeepSolo: Let transformer decoder with explicit points solo for text spotting. In *CVPR*, pages 19348–19357, 2023. 6
- [54] Xu-Cheng Yin, Wei-Yi Pei, Jun Zhang, and Hong-Wei Hao. Multi-orientation scene text detection with adaptive clustering. *IEEE TPAMI*, 37(9):1930–1937, 2015. 5
- [55] Wenwen Yu, Yuliang Liu, Wei Hua, Deqiang Jiang, Bo Ren, and Xiang Bai. Turning a clip model into a scene text detector. In *CVPR*, pages 6978–6988, 2023. 6, 7
- [56] Wenwen Yu, Yuliang Liu, Xingkui Zhu, Haoyu Cao, Xing Sun, and Xiang Bai. Turning a clip model into a scene text spotter. *arXiv:2308.10408*, 2023. 6, 7
- [57] Sangdoon Yun, Dongyoon Han, Seong Joon Oh, Sanghyuk Chun, Junsuk Choe, and Youngjoon Yoo. Cutmix: Regularization strategy to train strong classifiers with localizable features. In *ICCV*, pages 6023–6032, 2019. 1, 4, 8
- [58] Bowen Zhang, Yidong Wang, Wenxin Hou, Hao Wu, Jindong Wang, Manabu Okumura, and Takahiro Shinozaki. Flexmatch: Boosting semi-supervised learning with curriculum pseudo labeling. In *NeurIPS*, pages 18408–18419, 2021. 3
- [59] Chengquan Zhang, Borong Liang, Zuming Huang, Mengyi En, Junyu Han, Errui Ding, and Xinghao Ding. Look more than once: An accurate detector for text of arbitrary shapes. In *CVPR*, pages 10552–10561, 2019. 6
- [60] Hongyi Zhang, Moustapha Cisse, Yann N Dauphin, and David Lopez-Paz. mixup: Beyond empirical risk minimization. *arXiv:1710.09412*, 2017. 1, 4, 8
- [61] Zhen Zhao, Lihe Yang, Sifan Long, Jimin Pi, Luping Zhou, and Jingdong Wang. Augmentation matters: A simple-yet-effective approach to semi-supervised semantic segmentation. In *CVPR*, pages 11350–11359, 2023. 5, 9
- [62] Yiqin Zhu, Jianyong Chen, Lingyu Liang, Zhanghui Kuang, Lianwen Jin, and Wayne Zhang. Fourier contour embedding for arbitrary-shaped text detection. In *CVPR*, pages 3123–3131, 2021. 1, 3, 5, 6